ACS OMEGA

Open Access

http://pubs.acs.org/journal/acsodf

Article

Waste-Derived Carbon Nano-Onions for the Removal of Organic Dye from Wastewater and Phytotoxicity Studies

Diwakar Patel, Kumud Malika Tripathi,* and Ravi Kumar Sonwani*

Cite This: *ACS Omega* 2024, 9, 30834−30845

Read Online

ACCESS | Metrics & More | Article Recommendations

ABSTRACT: Dyes are extensively employed in industries, namely, textiles, cosmetics, paper, pharmaceuticals, tanning, etc. The effluent released from these industries contains various kinds of harmful dyes that adversely impact living beings and the environment due to their recalcitrant and toxic nature. In this study, an effort has been made to eliminate the methylene blue (MB) from wastewater using carbon nano-onions (CNOs) produced from waste frying oil (WFO) using an economical and eco-friendly wick pyrolysis method. The impact of process variables, namely, pH, temperature, process time, MB dye concentration, and adsorbent, was examined for optimum dye removal. The dye removal efficiency (RE) of 99.78% was obtained in 20 min under optimum conditions. The pseudo-second-order model demonstrated a better kinetic fitting with the experimental data. The Langmuir model represented the maximum adsorption capacity (q_{max}) of 43.11 ± 2.56 mg g^{-1}. The regeneration studies demonstrated that the CNOs achieved ∼99.6% MB dye removal over three cycles. *Brassica nigra* seeds irrigated in treated wastewater showed better growth (3.29 cm) than untreated dye wastewater, which confirms the environmental sustainability of the overall process.

1. INTRODUCTION

In the last few decades, synthetic dyes have been extensively employed in industries (e.g., carpet, cosmetics, pharmaceuticals, leather, etc.) to produce a wide range of products. Subsequently, these industries produce a significant amount of dye-containing wastewater.[1] Around 10−15% of the used dyes in industries are unreacted with fibers during dying processes and discharged ultimately into water bodies.[2] Around 2,80,000 tons per year of wastewater containing dyes are released into the environment globally.[3] Synthetic dyes are stable, complex aromatic structures and difficult to remove from the effluents.[4]

Dye-contaminated wastewater is highly colored with a high COD and BOD. Dyes in water bodies reduce the light intensity due to low sunlight penetration.[5] Synthetic dyes (e.g., methylene blue, methyl orange, etc.) are significant concerns among researchers due to their toxic and carcinogenic potential.[6,7] Synthetic dyes are visible in the aquatic system at low concentrations and exert aesthetic issues.[8] It is reported that methylene blue (MB) is extensively employed in various processes.[9] MB is resistant to degradation and poses potential risks to human health and the natural ecosystem.[10,11] MB-contaminated wastewater causes diarrhea, vomiting, allergic dermatitis, genetic mutations, and cancer.[12] Therefore, a suitable and cost-effective system is necessary to treat dyes containing wastewater.

In the past few decades, several measures have been explored to treat the dyes. Adsorption, photocatalysis, ozonation, advanced oxidation processes, and membranes are commonly applied to treat the dyes.[5,13−17] Among these, adsorption is associated with easy operation, low operating cost, and high removal efficiency (RE) of the contaminants.[18] Adsorption is a mass transfer phenomenon where the adsorbate, such as dye molecules, accumulates on an adsorbent material like activated carbon, biochar, or graphene composite.[19,20] It has been broadly employed to remove various contaminants from wastewater.[21,22] Adsorbents such as silica, zeolites, polymeric, biochar, and activated carbons have been extensively examined for dye removal.[23−27] Furthermore, researchers are currently looking for novel adsorbents with promising properties. Carbon-based materials, including graphene, carbon dots, carbon nano-onions (CNOs), etc., have recently gained significant popularity as adsorbents in various applications. Among all of the nanocarbons, CNOs receive pervasive attention for applications in water remediation because of their unique quasi-spherical multishelled structure and surface curvature.[28] CNOs show high efficacy due to their substantial

Received: April 13, 2024
Revised: June 21, 2024
Accepted: June 25, 2024
Published: July 5, 2024

surface area and mesoporous structure, which facilitate dye adsorption.

In this context, natural biomasses and waste materials (candle soot, flaxseed oil, vegetable gee, dead leaves, diesel soot, and fish waste) are the best alternative precursors to prepare CNOs. The application of frying oil in cooking generates a large amount of waste frying oil (WFO), which is generally discarded into the sink or water bodies (resulting in water pollution and energy loss), causing potential health issues.[29] It is expected that the WFO will further increase with population growth. To the best of our knowledge, CNOs produced from WFO have received very limited attention to remove hazardous synthetic dyes. According to Gunture et al., diesel soot-derived CNOs were employed to remove the MB dye from wastewater and achieved 247.78 mg/g of adsorption capacity for the MB dye.[30] In another study, modified CNOs were successfully employed to remove the MB dye from wastewater.[31]

A straightforward, one-step, economical, high-yielding, and eco-friendly technique has been employed to synthesize CNOs with excellent adsorption performance and for water remediation. The impact of process variables, namely, dose of CNOs, pH, MB concentration, process time, and temperature, was studied to treat the MB dye. The kinetics studies were performed by using isotherm models. Moreover, phytotoxicity was carried out to investigate the further potential of treated wastewater in plantations.

2. MATERIALS AND METHODS

2.1. Chemicals. Methylene blue (MB) dye ($C_{16}H_{18}ClN_3S\cdot 3H_2O$; M.W. = 373.9 g mol^{-1}) was purchased from Sigma-Aldrich (India). The simulated wastewater was prepared by adding the MB dye in deionized water. The serial dilution technique was employed to prepare dye solution for the experiments. The pH of simulated wastewater was maintained by adding 0.1 N hydrochloric acid and 0.1 N sodium hydroxide.

2.2. Synthesis of CNOs. WFO was employed as a feed source to synthesize the CNOs. WFO was collected from the hostel premises of the IIPE, Visakhapatnam, India. Initially, WFO was filtered through a regular strainer mesh to remove the suspended impurities. After that, CNOs were synthesized using the cotton wick combustion technique. It resulted in the formation of black carbon soot, which was further collected in an inverted earthen lamp. The obtained soot was heated at 600 °C in a furnace (I-therm AI-7481) to remove unburnt oil and loosely bonded carbons. The process flow diagram to synthesize the CNOs and their application in the MB dye removal is depicted in Figure 1.

2.3. Batch Studies. The simulated wastewater enriched with MB was employed for the adsorption studies. In the batch mode adsorption study, 50 mL of water sample was added in a 100 mL beaker and stirred at 300 rpm (Neuation istir HP550 Prime). The studies were conducted to optimize the operating parameters, namely, time, MB concentration, pH, CNO dosage, and temperature. The effect of contact time (1 to 40 min) was studied at 20 mg L^{-1} of MB and 1.0 g L^{-1} of CNOs. Once the optimum time was reached, the effect of CNOs with varying amounts of 0.25−2.0 g L^{-1} was studied under similar conditions. The impact of the initial MB dye (10−100 mg L^{-1}) was evaluated under optimum contact time and adsorbent. Similarly, the effect of pH (4.0−10) was studied under optimum contact time, adsorbent dose, and MB concentration.

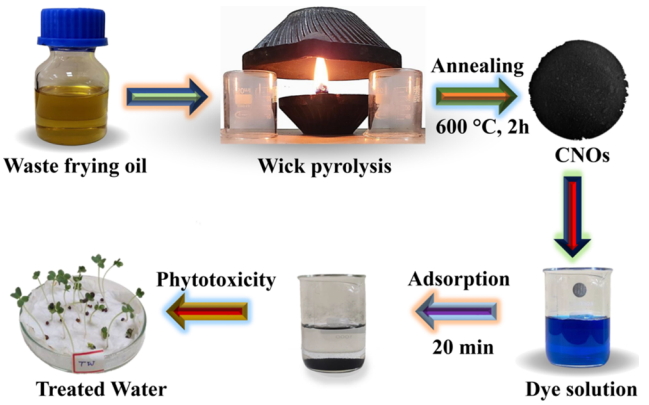

Figure 1. Process flow diagram to synthesize CNOs and their application in MB dye removal.

Further, temperature was changed from 20 to 50 °C under optimum contact time, pH, and adsorbent.

The samples were collected at different periods to estimate the efficacy of the CNOs in removing MB from wastewater. The samples were centrifuged (Coslab CLE-129NM) at 4000 rpm to remove the adsorbent. The RE and adsorption capacity were estimated using the following equations.

$$\text{removal efficiency (RE)} = \left(\frac{C_0 - C_t}{C_0}\right) \times 100 \quad (1)$$

$$\text{adsorption capacity } (q_e) = \left(\frac{C_0 - C_t}{m}\right) V \quad (2)$$

where C_0 and C_t represent the MB concentrations (mg L^{-1}) at time = 0 and time = t, respectively. m shows the amount of CNO (g), q_e represents the adsorption capacity in equilibrium (mg g^{-1}), and V shows the working volume of the reactor (L). All of the studies were conducted in triplicates.

2.4. Characterization Techniques. MB was estimated by a ultraviolet−visible (UV−vis) spectrophotometer (UV3200, LabIndia Analytical Instruments Pvt., Ltd.) at 664 nm. A pH meter (Spectral lab Eco) was employed to measure the pH. The surface morphology of CNOs was examined using high-resolution transmission electron microscopy (HRTEM) (Tecnai FEI-F30) operated at 300 kV. The specific surface area was estimated using Brunauer−Emmett−Teller (BET) isotherms (MicrotracBEL Belsorp Max-II). Crystallographic details and disorders were analyzed by using X-ray diffraction patterns (XRD) (Rigaku MiniFlex 600) to analyze the structure of CNOs. The functional groups of CNOs were detected by the Fourier-transform infrared (FTIR) (Thermo Electron Scientific Nicolet iS5). The Raman spectrum was analyzed by a Raman spectrophotometer (WITec). X-ray photoelectron spectroscopy (XPS) spectrum was determined by an X-ray source (ULVAC-PHI X) to detect the binding stages of C and O and the chemical composition on the surface of CNOs.

2.5. pH Zero-Point Charge (pHzpc). At pHzpc, the surface of the material has an equal number of positive and negative charges. In this study, pHzpc is determined using a standard protocol.[32] Initially, 50 mL of 0.01 N NaCl was added to a 100 mL beaker. Further, the solution of different pH values (i.e., 01−11) was prepared using 0.1 N NaOH or HCl. Then, 0.15 g of CNOs was added to each pH solution and kept

https://doi.org/10.1021/acsomega.4c03570
ACS Omega 2024, 9, 30834−30845

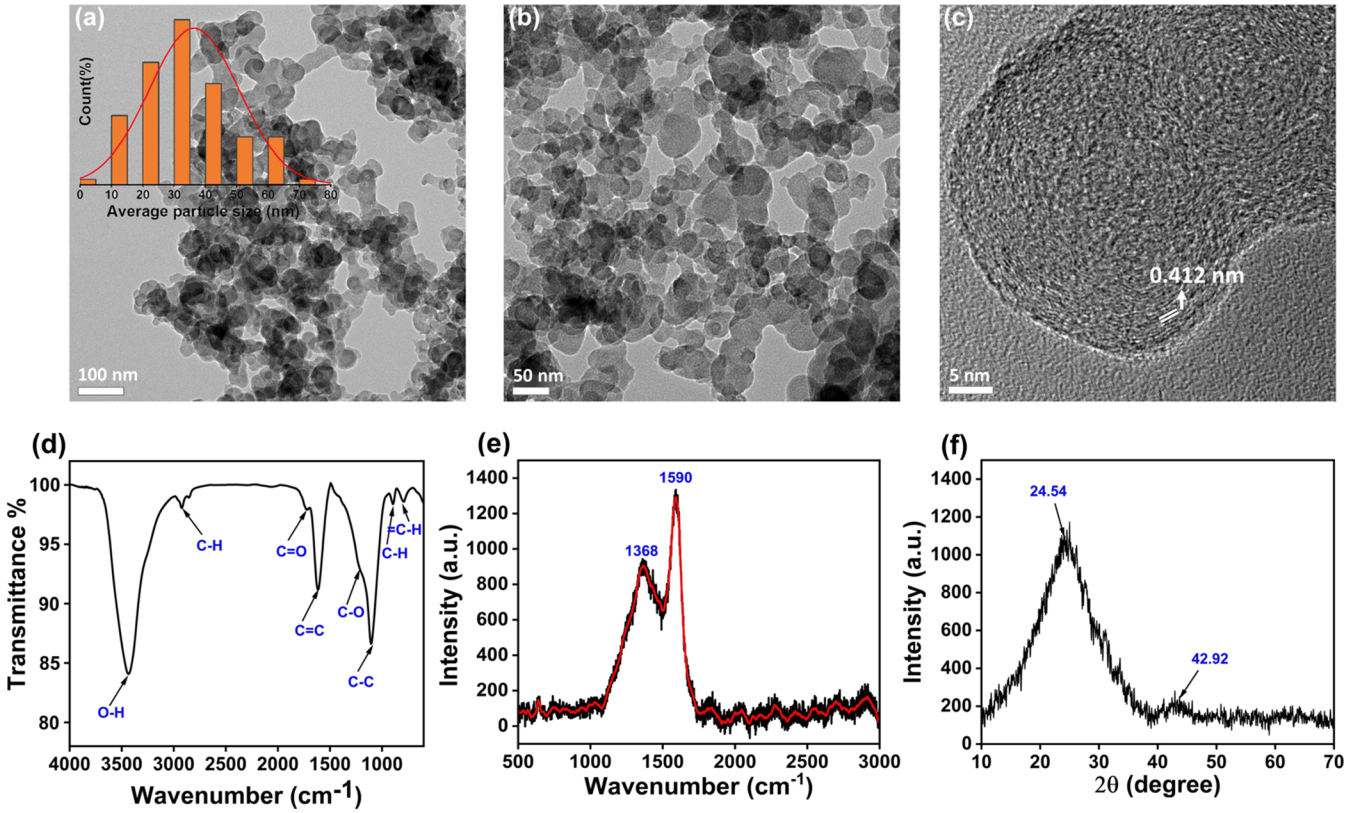

Figure 2. Morphological and structural analyses of the CNOs. (a, b) Low-resolution TEM images. (c) High-resolution TEM image. (d) FTIR spectrum of CNOs. (e) Raman spectrum of CNOs. (f) XRD pattern of the CNOs.

for 48 h under laboratory conditions. The final pH was measured to determine the pHzpc.

2.6. Adsorption Kinetics. The kinetic models, namely, pseudo-first-order (PFO), pseudo-second-order (PSO), Elovich, and intraparticle diffusion (IPD) models, were employed to study the adsorption isotherm. The nonlinear PFO model is shown by eq 3.

$$q_t = q_e(1 - e^{-k_1 t}) \tag{3}$$

where q_e represents the adsorption capacity at equilibrium (mg g^{-1}) and q_t adsorption capacity (mg g^{-1}) at time t. k_1 represents the rate constant (min^{-1}).

The PSO model is described by eq 4.

$$q_t = \frac{k_2 q_e^2 t}{1 + K_2 q_e t} \tag{4}$$

where k_2 (g mg^{-1} min^{-1}) represents rate constant pseudo-second-order model.

The Elovich adsorption kinetic model shows a linear correlation between the adsorption energy and the surface coverage. The Elovich model can be represented by eq 5.

$$q_t = \frac{1}{\beta} \ln(1 + \alpha\beta t) \tag{5}$$

where α shows the initial adsorption rate (mg g^{-1} min). β represents the desorption constant (g mg^{-1}). An IPD model is also applied to determine the diffusion mechanism occurring during adsorption.[33] This model is defined by subsequent eq 6.

$$q_t = k_p t^{0.5} + C \tag{6}$$

where K_p (mg g^{-1} $min^{-0.5}$) and C (mg g^{-1}) show IPD model constants. The models were fitted using Origin 2023 software, and all of the kinetic coefficients were calculated by analyzing the fitted data. The parameters such as coefficient of correlation (R^2), reduced chi-square (r-χ^2), and Akaike information criterion (AIC) are generally used to analyze the data fitting with various models.[34] The value of R^2 and r-χ^2 close to 1 shows that the data are well fitted with the model. Further, AIC is a numerical score that helps to identify the most suitable model. A lower AIC value supports the suitable model fitting.

2.7. Adsorption Isotherm Study. The adsorption isotherms help determine adsorbed molecules' distribution between the absorbent and adsorbate. Langmuir, Freundlich, Temkin, and Dubinin−Radushkevich (D−R) were employed for the adsorption isotherms study.[35] The simplified mathematical expression of the Langmuir isotherm is given as[36]

$$q_e = \frac{q_m K_L C_e}{1 + K_L C_e} \tag{7}$$

where q_m and K_L represent the maximum adsorption capacity (mg g^{-1}) of CNOs and the Langmuir constant (L mg^{-1}), respectively. The values of q_m and K_L were obtained by analyzing the nonlinear plot between q_e and C_e. The Freundlich isotherm explains heterogeneous nonideal and reversible adsorption. The simplified nonlinear mathematical expression of the Freundlich isotherm is given as[37]

$$q_e = K_F \cdot C_e^{1/n} \tag{8}$$

https://doi.org/10.1021/acsomega.4c03570
ACS Omega 2024, 9, 30834−30845

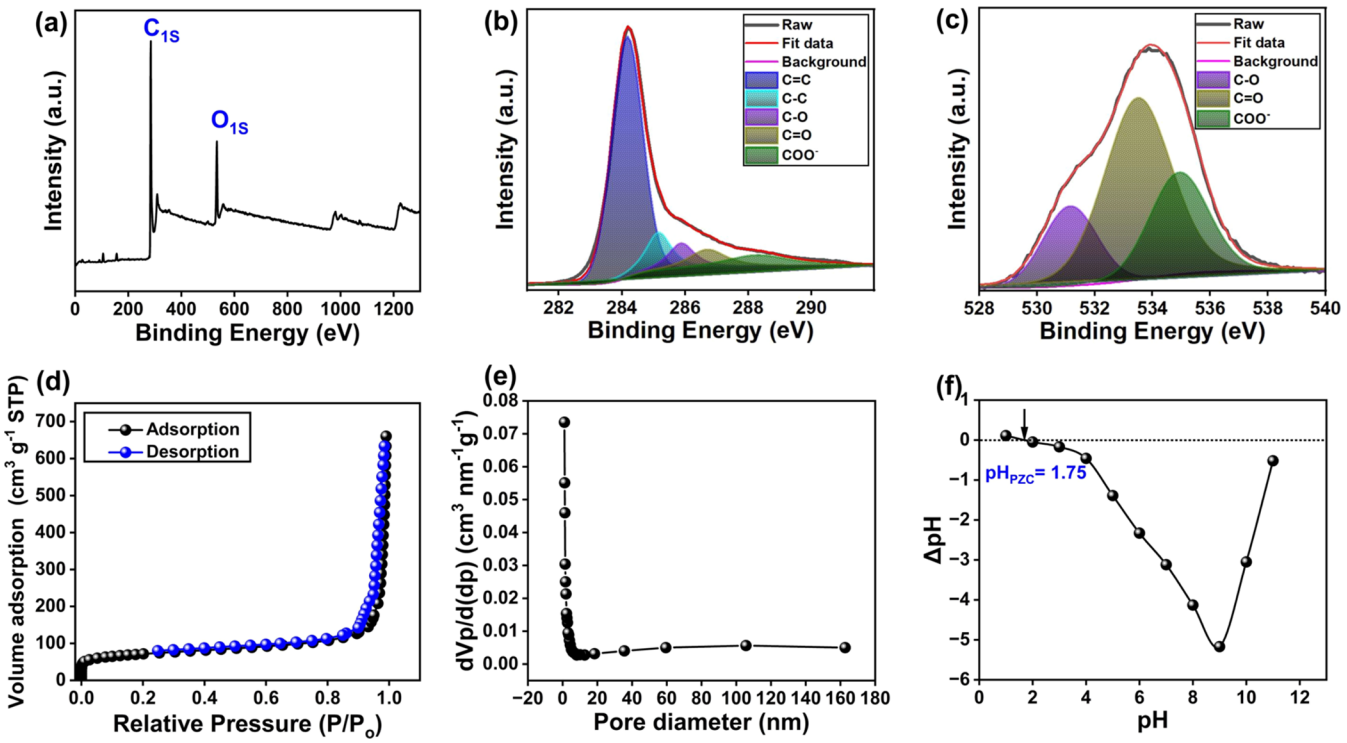

Figure 3. XPS spectra of CNOs: (a) wide-range scan spectrum, (b) C 1s scan spectrum, and (c) O 1s scan spectrum. (d) N_2 adsorption−desorption isotherm of CNOs. (e) Distribution of pore size CNOs. (f) pH_{pzc} of CNOs.

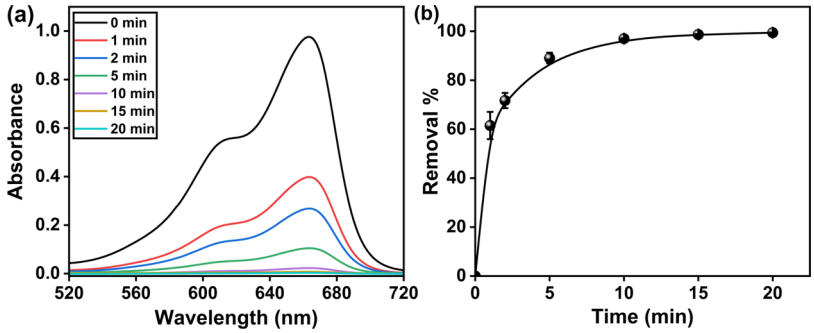

Figure 4. Effect of process time on (a) absorbance and (b) removal percentage of the MB dye.

where K_F ($(mg\ g^{-1})(L\ mg^{-1})^{1/n}$) and n represent the Freundlich isotherm constants. The adsorption is beneficial and feasible when the value of n is >1. Further, Temkin isotherm was also employed for isotherm study eq 9.[38]

$$q_e = \frac{RT}{B_T} \ln K_T + \frac{RT}{B_T} \ln C_e \tag{9}$$

where $B = RT\ B_T^{-1}$. B_T is the Temkin constant (joules mol^{-1}) and K_T denotes the equilibrium binding constant (L g^{-1}). The D−R isotherm eq 10 is a well-known and frequently utilized model in the field of adsorption.[39] The D−R isotherm model operates under the concept that adsorption primarily involves the occupation of micropores and accumulation of adsorbate layers on the surface of pore walls eqs 10 and 11.

$$q_e = q_{D-R} \exp\left(-K_{D-R}\left[RT \ln\left(1 + \frac{1}{C_e}\right)\right]\right) \tag{10}$$

$$\ln(q_e) = \ln(q_{D-R}) - K_{D-R}\epsilon^2 \tag{11}$$

where q_{D-R} (mg g^{-1}) and K_{D-R} ($mol^2\ kJ^{-2}$) represent the D−R constants. ε is the Polanyi potential, which is expressed by eq 12.[40]

$$\varepsilon = RT \ln\left(1 + \frac{1}{C_e}\right) \tag{12}$$

where R is the gas constant (J mol^{-1} K^{-1}) and T is the temperature (K). The mean adsorption energy (E) is calculated by eq 13.

$$E = \frac{1}{\sqrt{2K_{D-R}}} \tag{13}$$

2.8. Reusability and Phytotoxicity Studies. The capability to recycle and regenerate adsorbents is essential for their practical implementation. The materials that show better regeneration potential can minimize the disposal issues of exhausted adsorbents and subsequently reduce the overall cost of the treatment process. Three adsorption−desorption cycle studies were carried out to estimate the reusability of

https://doi.org/10.1021/acsomega.4c03570
ACS Omega 2024, 9, 30834−30845

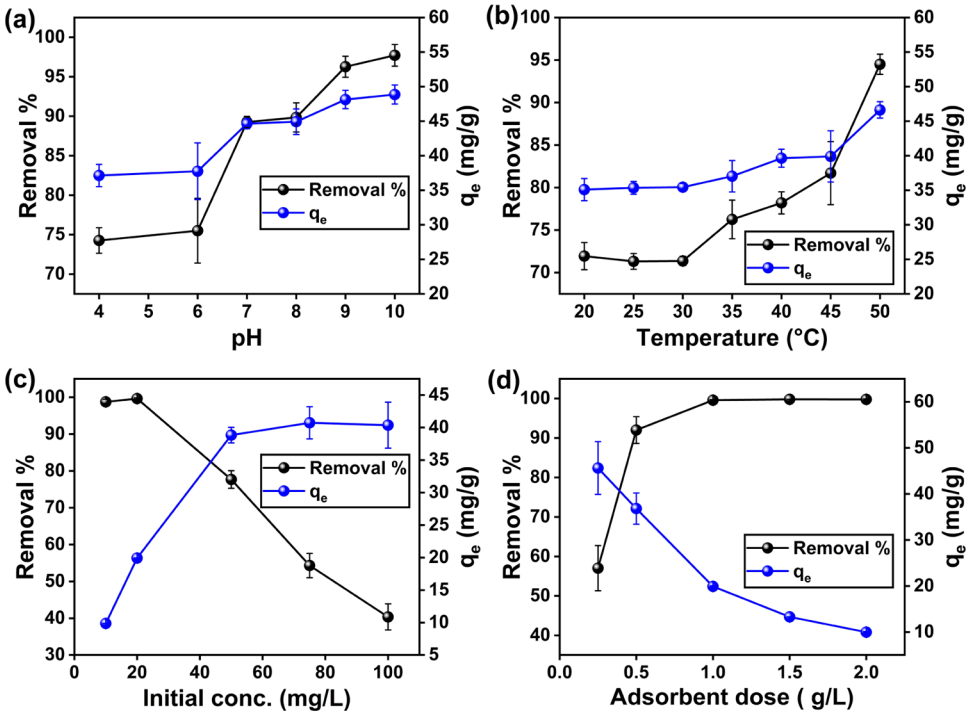

Figure 5. Effect of process parameters on the adsorption of MB: (a) pH, (b) temperature, (c) MB dye, and (d) adsorbent dose.

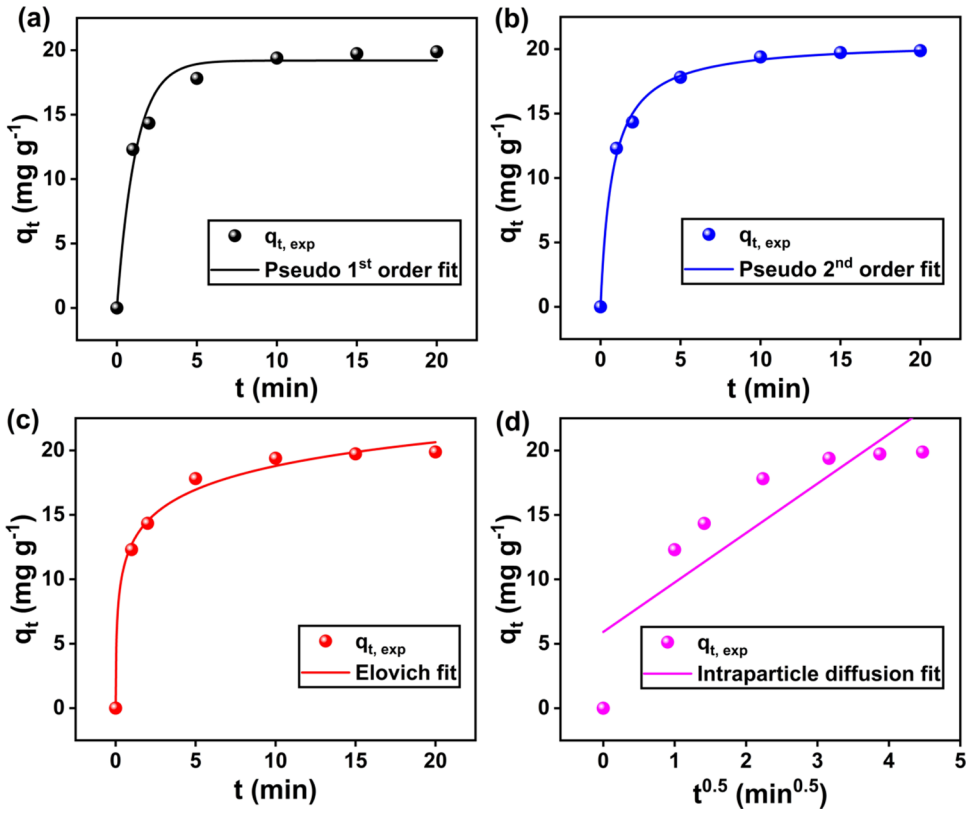

Figure 6. Adsorption kinetic plots: (a) pseudo-first-order kinetic, (b) pseudo-second-order kinetic, (c) Elovich kinetic model, and (d) linear fitting of the intraparticle diffusion models (C_0 = 20 mg L^{-1}, m = 50 mg, t = 20 min, T = 30 ± 2.0 °C, pH = 6.5, and stirrer speed = 300 rpm).

CNOs. In this work, a thermal regeneration method was used to regenerate the CNOs. The saturated CNOs after the adsorption of the MB dye were heated at 600 °C for 2 h.

A phytotoxicity study was carried out to explore the potential application of treated wastewater in the irrigation of agricultural crops. *Brassica nigra* (mustard) seeds were used for the phytotoxicity study. Initially, 20 seeds of *B. nigra* were taken into three different Petri dishes (100 mm × 15 mm). After that, the seeds were irrigated separately with equal amounts of deionized water, untreated dye-containing water,

https://doi.org/10.1021/acsomega.4c03570
ACS Omega 2024, 9, 30834−30845

and treated water. These dishes were kept for 7 days under laboratory conditions (30 ± 2.0 °C) for the growth of seeds. Further, the seeds were irrigated with deionized water, untreated dye-containing water, and treated water at regular time intervals.

3. RESULTS AND DISCUSSION

3.1. Characterization Techniques. The morphologies of CNOs are represented in Figure 2. It was observed that the particles of CNOs are dispersed and quasi-spherical. Most of the sizes of particles were found to be in the range of 20−40 nm (Figure 2a,b). The pyrolysis of frying oil at high temperatures leads to the formation of spheroidal. This spheroidal structure interconnects with other structures and forms a graphitized carbon core.[41] Figure 2c demonstrates concentric graphitic interplanar fringes spaced at 0.412 nm, exhibiting numerous defects. The annealing process caused the transition from sp^3 carbon to more sp^2 carbon atoms, reorganizing the concentric graphitic layers.[42]

Table 1. Summary of Fitted Kinetic Models for the Adsorption of the MB Dye onto CNOs[a]

model	equation	parameter	value
PFO	$q_t = q_e(1 - e^{-k_1 t})$	$q_{e,exp}$	19.88
		$q_{e,cal}$ (mg g^{-1})	19.20 ± 0.54
		k_1 (min^{-1})	00.85 ± 0.11
		r-χ^2	1.1115
		R^2	0.9818
		AIC	12.3847
PSO	$q_t = \frac{k_2 q_e^2 t}{1 + k_2 q_e t}$	$q_{e,cal}$ (mg g^{-1})	20.62 ± 0.27
		k_2 (g mg^{-1} min^{-1})	0.065 ± 0.006
		r-χ^2	0.1526
		R^2	0.9975
		AIC	−1.5153
Elovich	$q_t = \frac{1}{\beta}\ln(1 + \alpha\beta t)$	α (mg g^{-1} min)	311.85 ± 155.78
		β (g mg^{-1})	0.376 ± 0.034
		r-χ^2	0.37425
		R^2	0.9939
		AIC	4.7649
IPD	$q_t = k_p t^{0.5} + C$	k_p (mg g^{-1} $min^{-0.5}$)	3.84 ± 0.97
		C	5.92 ± 2.68
		R^2	0.7562

[a]PFO: pseudo-first-order; PSO: pseudo-second-order; IPD: intraparticle diffusion.

FTIR spectrum demonstrates the analysis of functional groups on the surface of CNOs (Figure 2d). The peaks observed around 3434 and 1711 cm^{-1} demonstrate the stretching and vibration of O−H and C═O, respectively. Together, these peaks indicate the stretching vibration of COOH.[43] A peak found at ∼1613 cm^{-1} indicates the occurrence of sp^2 aromatic carbons (C−C). The peaks observed at ∼1197 and ∼1442 cm^{-1} indicate the vibrations of C−C and C−O, respectively. The collective weak peaks observed at ∼2922 cm^{-1} result from alkyl C−H bond stretching vibrations. The peaks around 897 and 799 cm^{-1} were associated with the out-of-plane C−H and ═C−H bending vibrations, respectively.[44]

The characteristic disorder (D band) and graphitic (G band) peaks were found at 1368 and 1590 cm^{-1}, respectively, using the Raman spectrum (Figure 2e).[45] D band showed that defects in the structure arise due to the A_{1g} vibrational mode, whereas the G peak showed that the graphitic nature of carbon arises due to the E_{2g} vibrational mode of aromatic C═C bond stretching. The CNOs show a high I_D/I_G value of ∼1.21, which suggests high structural defect and low graphitization. The powder XRD patterns of the CNOs (Figure 2e) exhibit two peaks at 2θ = 24.54 and 42.92°, corresponding to the (002) and (101) reflections of graphitic planes. There are no other distinctive peaks that show the high purity of the CNOs.[44]

The XPS spectrum is analyzed to detect the binding stages of C and O and the chemical composition on the surface of CNOs. Figure 3a displays the full XPS survey scan and shows two peaks, C 1s (83.33%) and O 1s (16.1%), centered at 285.08 and 534.08 eV, respectively. C 1s was associated with five characteristic peaks at 284.18, 285.18, 285.88, 286.68, and 288.38 eV of binding energies, which indicates the C═C, C−C, C−O, C═O, and COO^- functional groups, respectively.[46] The deconvoluted spectrum of O 1s given in Figure 3c shows three peaks at different binding energies of 531.15, 533.5, and 534.93 eV, corresponding to the C−O, C═O and COO^- functional groups.[47]

Figure 3d illustrates type IV adsorption and desorption isotherm with 236 m^2 g^{-1} of surface area. The BJH experimental isotherm was applied for the estimation of the pore size of the CNOs, revealing an average pore diameter of 16.5 nm. This observation strongly indicates that the CNOs exhibit characteristics of a mesoporous adsorbent (Figure 3e).[48]

3.2. Optimization Studies. *3.2.1. Effect of Process Time.* The MB dye removal efficiency (RE) with respect to the process time is represented in Figure 4. Initially, the MB dye RE was increased with process time and reached 98.6% in 15 min. With further increase in the processing time, not much significant improvement was observed. The maximum RE of 99.4% was obtained in 20 min. The presence of more available sites leads to a higher MB dye RE.[49] However, with the increase in process time, the adsorbent sites were filled with the adsorbate (i.e., MB) and subsequently reduced the MB dye RE.

3.2.2. Zero-Point Charge (pHzpc) and Effect of pH. A plot between the ΔpH and the initial pH of CNOs is represented in Figure 3f. The pHzpc of the CNOs was found to be 1.75 at the intersection of the curve. It indicates that the material surface behaves negatively charged beyond 1.75 pH of the solution and is suitable for adsorbing the positively charged ions (cations). Below 1.75 pH, the material becomes positively charged and more suitable for the adsorption of negatively charged ions (anions). Boumediene et al. prepared the orange peel adsorbent to remove methylene blue.[32] It was found that the material was suitable to adsorb the cation and anion molecules above and below pHzpc (1.75), respectively. In the pH effect study, the MB dye RE and adsorption capacity were enhanced with increasing pH. The REs of 74.2 and 97.7 were found at pH 4 and 10, respectively. Similarly, the adsorption capacities (ACs) were found to be 38.1 to 48.9 mg g^{-1} at pH 3.0 and 10, respectively (Figure 5a). It was due to the negative pHzpc of the CNOs. Since CNOs have a low pHzpc, this causes a rise in adsorption with the increasing pH. CNOs exhibiting a negatively charged surface after pH 1.75 were more attracted to cationic MB dye particles.

3.2.3. Effect of Temperature. Temperature was varied from 20 to 50 °C to absorb the MB dye onto CNOs (Figure 5b). The MB dye RE was enhanced with increasing the temperature. The MB dye removal efficiencies were 71.9 and 94.5% at

https://doi.org/10.1021/acsomega.4c03570
ACS Omega 2024, 9, 30834−30845

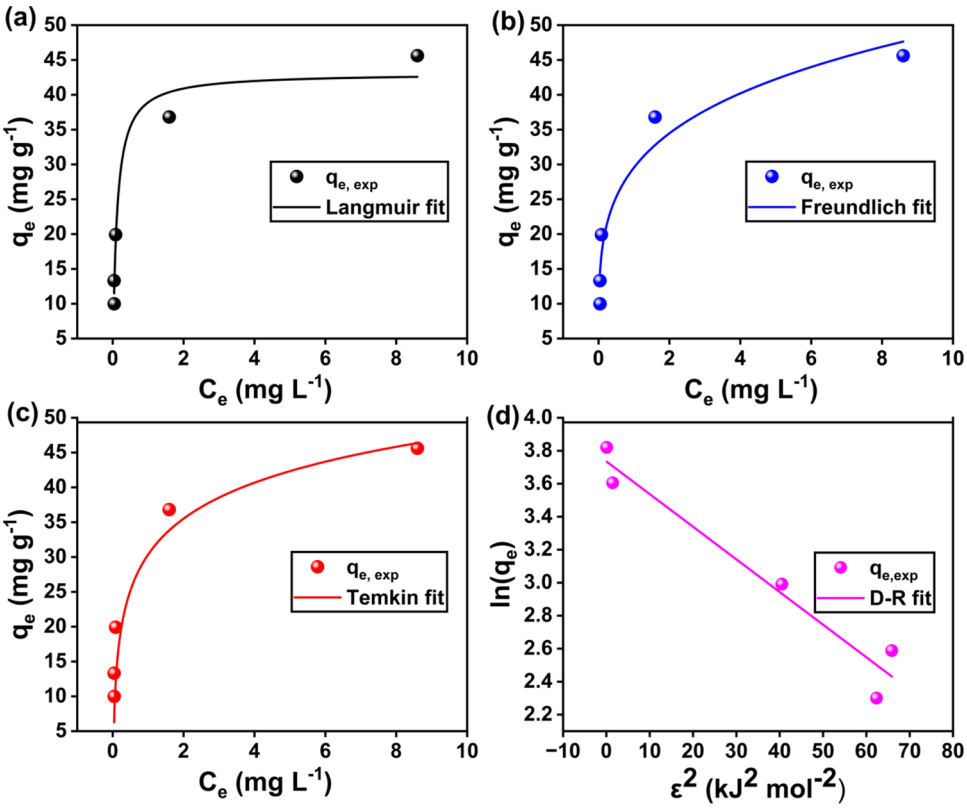

Figure 7. Fitting of experimental data with isotherm models: (a) Langmuir, (b) Freundlich, (c) Temkin, and (d) linear fitting of D−R.

Table 2. Summary of the Adsorption Isotherm Models

model	equation	parameter	value
Langmuir model	$q_e = \frac{q_m K_L C_e}{1 + K_L C_e}$	q_{max} (mg g^{-1})	43.11 ± 2.56
		K_L (L mg^{-1})	9.24 ± 2.15
		R^2	0.9664
		AIC	39.2873
Freundlich model	$q_e = K_F \cdot C_e^{1/n}$	K_F (mg g^{-1})(L mg^{-1})$^{1/n}$	29.55 ± 2.11
		n	4.50
		R^2	0.9451
		AIC	41.7355
Temkin model	$q_e = \frac{RT}{B_T} \ln K_T + \frac{RT}{B_T} \ln C_e$	B_T (J mol^{-1})	332.96
		K_T (L mg^{-1})	59.12
		R^2	0.9806
		AIC	36.7140
D−R model	$\ln(q_e) = \ln(q_{D-R}) - K_{D-R}\epsilon^2$	K_{D-R} (mol^2 kJ^{-2})	0.0198
		q_{D-R} (mg g^{-1})	41.89
		E (kJ mol^{-1})	5.02
		R^2	0.9489

20 to 50 °C, respectively. The better RE at higher temperatures was due to the fast mobility of dye particles toward adsorbent sites. The higher temperature leads to a rise in dye adsorption on CNOs, supporting the endothermic adsorption process.

3.2.4. Effect of MB Dye Concentration. The adsorption process was performed by adding 50 mg of adsorbent to the dye solution and kept for 20 min of process time. The RE of the dye at different concentrations is shown in Figure 5c. Initially, ∼100% dye removal efficacy was obtained with 20 mg L^{-1} MB dye. The RE was reduced with increasing dye and reached 40.4% at 100 mg L^{-1}. The saturation of the active adsorbent sites with MB dye molecules may be responsible for the reduction of RE at higher concentrations.

In contrast, the AC was significantly increased with the increase in the MB dye from 20 to 50 mg L^{-1}. After that, no significant improvement was observed because of the absorbent saturation. The equilibrium AC of 40.4 mg g^{-1} was obtained at 75 mg L^{-1} of MB. This is attributed to the limited availability of adsorbent surfaces at a high concentration of MB dye. According to Pathania et al., at higher concentrations, dye RE was reduced with the gradual occupying active site of adsorbent by adsorbate (i.e., MB).[49]

3.2.5. Effect of Adsorbent Dose. The variation in the MB dye RE with respect to the adsorbent amount is shown in Figure 5d. The MB dye RE was enhanced with increasing CNOs from 0.25 to 1.0 g due to the increased adsorption

https://doi.org/10.1021/acsomega.4c03570
ACS Omega 2024, 9, 30834−30845

Table 3. Comparison of Adsorption Capacity of CNOs with Carbon Nanomaterials Reported in the Previous Literature[a]

adsorbent	dye	removal %	maximum adsorption capacity (mg g^{-1})	adsorption conditions	ref
cellulose/clay composite I	drimarine yellow HF-3GL dye	88.64	48.97	CT: 60 min, pH: 2, *T*: 30 °C, AD: 2 g L^{-1}, IC: 10 mg L^{-1}	Kausar et al.[52]
clay/PNIPAm	crystal violet		12.9	CT: 12 h, pH: 8.9, *T*: 25 °C, AD: -, IC: 30 mg L^{-1}	Zhang et al.[53]
halloysite nanotubes	safranin O	98	37.518	CT: 6 h, pH: 4, *T*: 30 °C, AD: 10^4 g L^{-1}, IC: 100 mg L^{-1}	Shaik et al.[54]
poly(methacrylic acid-*co*-acrylamide)/cloisite 30B nanocomposite hydrogel	methylene blue	98.57	32.83	CT: 60 min, pH: 8, *T*: 25 °C, AD: 1.5 g L^{-1}, IC: 10 mg L^{-1}	Safarzadeh et al.[55]
magnesite-halloysite nanocomposite	methylene blue	99.66	0.7079	CT: 60 min, pH: 2, *T*: 25 °C, AD: 40 g L^{-1}, IC: 10 mg L^{-1}	Ngulube et al.[56]
multiwall carbon nanotubes (MWCNTs)	reactive blue 116 dye	80	71.05	CT: 60 min, pH: 12, *T*: RT, AD: 3 g L^{-1}, IC: 100 mg L^{-1}	De Benedetto et al.[57]
magnetic activated carbon	sunset yellow		22.31	CT: 240 min, pH: 5.88, *T*: -, AD: 1 g L^{-1}, IC: 100 mg L^{-1}	Cazetta et al.[58]
Fe_3O_4/MgO nanoparticles	amaranth dye	96	37.98	CT: 60 min, pH: 9, *T*: 35 °C, AD: 1 g L^{-1}, IC: 24.8 mg L^{-1}	Salem et al.[59]
Fe_2O_3 nanoparticles	reactive blue	91	34.89	CT: 80 min, pH: 3, *T*: 65 °C, AD: 0.2 g L^{-1}, IC: 200 mg L^{-1}	Noreen et al.[60]
carbon nano-onions (CNOs)	methylene blue	99.4	43.11	CT: 20 min, pH: 6.5, *T*: 30 °C, AD: 1 g L^{-1}, IC: 20 mg L^{-1}	this work

[a]IC: initial concentration; CT: contact time; AD: adsorbent dose; *T*: temperature.

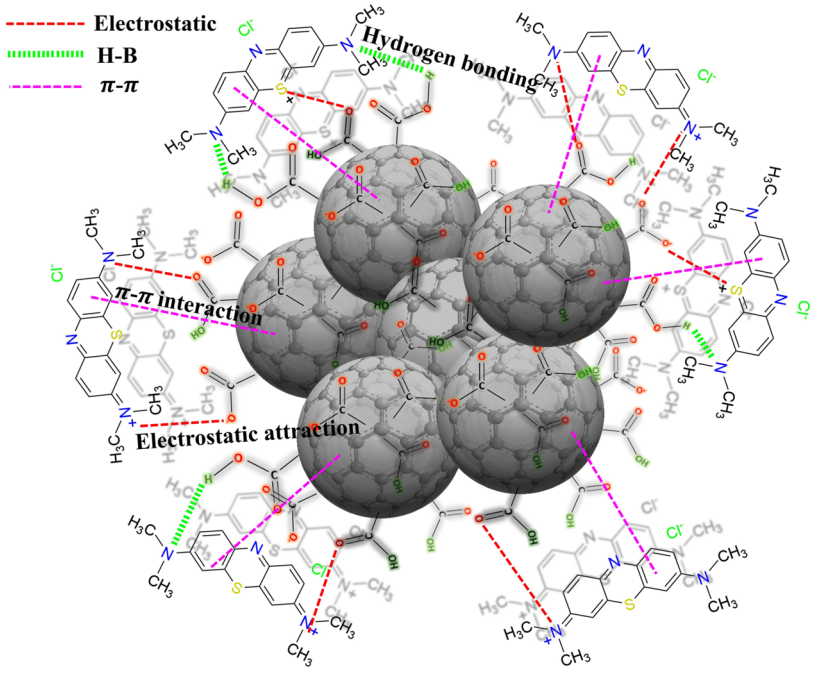

Figure 8. Proposed mechanism for MB dye adsorption onto the CNOs.

surface area and functional groups. No significant improvements were observed by further increasing the adsorbent dose, and the dye removal percentage remained almost constant. The dye removal efficiencies of 57, 92, 99.5, 99.8, and 99.78% were estimated at 0.25, 0.5, 1.0, 1.5, and 2.0 g L^{-1} of adsorbent doses, respectively. The AC of 45.62 mg g^{-1} was obtained at 0.25 g L^{-1} of the adsorbent dose. Low adsorbent doses may not have enough active sites to capture all dye molecules, resulting in lower adsorption efficiency.[50]

3.3. Adsorption Kinetic. The data fitted with various models (i.e., PFO, PSO, and Elovich models) are represented in Figure 6a–c. The data plotted with the IPD model are shown in Figure 6d. The constants obtained with the fitting of models, namely, PFO, PSO, Elovich, and IPD models, are summarized in Table 1. The highest R^2 value of 0.997 was achieved with the PSO model. Additionally, the PSO model exhibited lower values of r-χ^2 and AIC than the other models. The values of $q_{t.cal}$ and k_2 were found to be 20.62 mg g^{-1} and 0.065 g mg^{-1} min^{-1}, respectively, using PSO. The value of *C* in the IPD model was more than zero, which supported the fact that the diffusion of dye molecules into CNOs was not the rate-determining step.[51]

3.4. Adsorption Isotherm Study. The experimental data fitted with the models are represented in Figure 7. The values q_{max} and K_L were obtained to be 43.11 ± 2.5 and 9.24 ± 2.1, respectively, using the Langmuir isotherm (Table 2). Similarly, using the Freundlich isotherm, K_F and *n* were estimated to be 29.55 ± 2.1 and 4.5, respectively. The R^2 values of 0.966 and 0.945 were obtained for the Langmuir and Freundlich isotherms, respectively. The value of *n* (>1) suggested

https://doi.org/10.1021/acsomega.4c03570
ACS Omega 2024, 9, 30834−30845

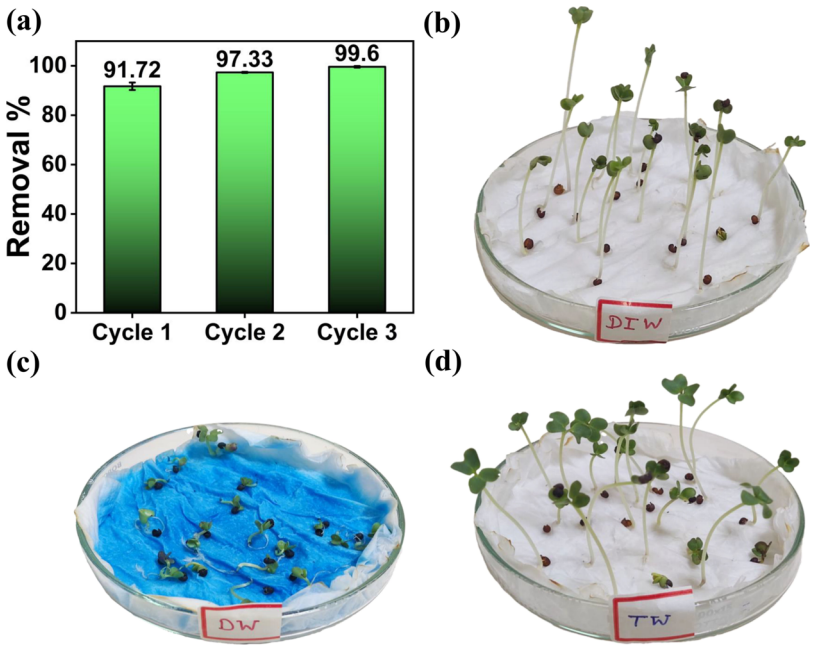

Figure 9. (a) Regeneration study of CNOs. Germination of *B. nigra* seeds in (b) deionized water, (c) untreated wastewater (dye concentration 20 mg L^{-1}), and (d) treated wastewater.

supported the adsorption of dye into CNOs was favorable.[38] The Langmuir isotherm represented better fitting with experimental data and supported the monolayer adsorption. This implies a strong affinity between the adsorbate and the adsorbent. The values obtained from the Temkin isotherm model for K_T and B_T were 59.12 L mg^{-1} and 0.333 kJ mol^{-1}, respectively, with an R^2 value of 0.9806 (Table 2). The adsorption energy derived by the D−R model was 5.02 kJ mol^{-1}, suggesting the physisorption of the MB dye onto CNOs. The adsorption capacity of CNOs was compared with those of the other nanomaterial adsorbents and is reported in Table 3.

3.5. Adsorption Mechanism. The adsorption mechanism of the adsorbate molecule onto the adsorbent is a challenging task because various factors work simultaneously between the interactions of adsorbate and adsorbent. The interactions and adsorption equilibrium may be influenced by factors such as surface chemistry, textural properties, functional group present on the surface of the adsorbent, molecular structure of the adsorbate, etc.[58] The mechanism for the adsorption of the MB dye onto the CNOs was hypothesized based on the FTIR analysis and the molecular structure of the MB dye (Figure 8). The experimental data was analyzed using various kinetic and isotherm models. The outcomes indicate that the PSO model provides the best fit, while the D−R model suggests physisorption. The pHzpc revealed the anionic nature of CNOs at pH 6.5, while the MB dye molecules exhibited a positive charge. Thus, this research demonstrated the presence of electrostatic attraction between CNOs and dye molecules. The electrostatic attraction may be present between the electronegative element (oxygen) of CNOs and the positive charge present in the MB dye molecule. The positive charge in the MB dye molecule was labile due to resonance and possessed by nitrogen and sulfur atoms. Therefore, there are multiple attraction points present for one MB dye molecule. Along with this electrostatic attraction, there is the possibility of intermolecular hydrogen bond formation (H−B) and $\pi-\pi$ attraction between the aromatic ring system of the MB dye and the π electron cloud of CNOs.

3.6. Reusability of CNOs and Phytotoxicity Study of Treated Wastewater. The regeneration of CNOs helps to minimize the cost of the adsorption process and makes it more environmentally sound. The thermally regenerated CNOs were employed to remove the MB dye from wastewater at 50 mg L^{-1}. The removal percentage was increased with each cycle, and 99.6% of the MB dye RE was achieved up to three cycles under optimum conditions, indicating that CNOs have good regeneration potential (Figure 9a). This improvement is attributed to the expansion of micro and meso pores in the CNOs, which enhances adsorption capacity. During regeneration, the adsorbate molecules (MB dye) undergo partial oxidation, creating larger pores when the adsorbent is heated to 600 °C with limited oxygen.[61] It supports the reusability of CNOs in dye removal and minimizes the cost of CNO preparation and the spent absorbent. The regeneration potential of eggshell membrane-based adsorbent was evaluated to remove the Reactive Red 120 dye from wastewater.[62] They reported that the adsorption efficiency decreased to around 67% after three cycles. However, in the present work, CNOs exhibited higher RE to remove the dye under the same regeneration cycle.

B. nigra seeds were grown in deionized water, untreated dye wastewater, and treated wastewater, as shown in Figure 9b−d. It was found that the seeds irrigated with deionized water exhibited a shoot length of 3.68 cm. However, a better average shoot length of 3.29 cm was observed when the seeds were irrigated with treated water than when the seeds were irrigated with untreated dye-containing water (1.18 cm). The lower shoot length in untreated wastewater may be due to a high concentration of MB dye molecules, which adversely affects the growth of *B. nigra* seeds. *Zea mays* and *Vigna unguiculata* showed better germination in MB dye-treated wastewater.[63] Similarly, Sonwani et al. conducted a phytotoxic study with

https://doi.org/10.1021/acsomega.4c03570
ACS Omega 2024, 9, 30834−30845

Vigna radiata seeds and reported that the seeds germinated in treated wastewater achieved 4.95 times better growth.[64]

4. CONCLUSIONS

CNOs were synthesized using WFO in a sustainable manner and facile room-temperature synthesis process. They were employed to remove recalcitrant and toxic MB dye-containing wastewater. CNOs were highly influential in achieving a ∼99.78% MB dye removal efficiency within 20 min. The adsorption kinetics were estimated using various kinetic models, and it was observed that the PSO model provided a better fit with an R^2 value of 0.9975. The equilibrium studies used Langmuir, Freundlich, Temkin, and D−R models. Among these, the Langmuir isotherm exhibited a better fit to the experimental data with a maximum AC of 43.11 mg g^{-1}. The synthesized adsorbent exhibited excellent regeneration potential and achieved 99.6% MB dye RE up to three cycles. The phytotoxicity study supported that the *B. nigra* seeds grown in treated wastewater improved the average shoot length of 3.29 cm compared to untreated dye wastewater (1.18 cm). CNOs (i.e., adsorbent) derived from WFO may offer an efficient and economical route to remove the dyes from wastewater, and treated wastewater may be further explored for irrigation of agricultural crops.

AUTHOR INFORMATION

Corresponding Authors

Kumud Malika Tripathi − *Department of Chemistry, Indian Institute of Petroleum and Energy, Visakhapatnam 530003 Andhra Pradesh, India;* orcid.org/0000-0002-9440-2320; Email: kumud20010@gmail.com

Ravi Kumar Sonwani − *Department of Chemical Engineering, Indian Institute of Petroleum and Energy, Visakhapatnam 530003 Andhra Pradesh, India*; Email: ravikumar.che@iipe.ac.in

Author

Diwakar Patel − *Department of Chemistry, Indian Institute of Petroleum and Energy, Visakhapatnam 530003 Andhra Pradesh, India;* orcid.org/0009-0004-6535-0607

Complete contact information is available at: https://pubs.acs.org/10.1021/acsomega.4c03570

Notes

The authors declare no competing financial interest.

ACKNOWLEDGMENTS

The authors thankfully acknowledge the Indian Institute of Petroleum and Energy (IIPE), Visakhapatnam, India, for providing laboratory facilities and an Institute Research Grant (IIPE/DoRD/IRG/018) to execute the work.

REFERENCES

(1) Rather, L. J.; Akhter, S.; Hassan, Q. P. Bioremediation: Green and Sustainable Technology for Textile Effluent Treatment. In *Sustainable Innovations in Textile Chemistry and Dyes*; Muthu, S. S., Ed.; Springer: Singapore, 2018; pp 75−91.

(2) Yaseen, D. A.; Scholz, M. Textile Dye Wastewater Characteristics and Constituents of Synthetic Effluents: A Critical Review. *Int. J. Environ. Sci. Technol.* **2019**, *16*, 1193−1226.

(3) Sonwani, R. K.; Swain, G.; Jaiswal, R. P.; Singh, R. S.; Rai, B. N. Moving Bed Biofilm Reactor with Immobilized Low-Density Polyethylene−Polypropylene for Congo Red Dye Removal. *Environ. Technol. Innovation* **2021**, *23*, No. 101558.

(4) Giri, B. S.; Sonwani, R. K.; Varjani, S.; Chaurasia, D.; Varadavenkatesan, T.; Chaturvedi, P.; Yadav, S.; Katiyar, V.; Singh, R. S.; Pandey, A. Highly Efficient Bio-Adsorption of Malachite Green Using Chinese Fan-Palm Biochar (Livistona Chinensis). *Chemosphere* **2022**, *287*, No. 132282.

(5) Vikrant, K.; Giri, B. S.; Raza, N.; Roy, K.; Kim, K.-H.; Rai, B. N.; Singh, R. S. Recent Advancements in Bioremediation of Dye: Current Status and Challenges. *Bioresour. Technol.* **2018**, *253*, 355−367.

(6) Brüschweiler, B. J.; Merlot, C. Azo Dyes in Clothing Textiles Can Be Cleaved into a Series of Mutagenic Aromatic Amines Which Are Not Regulated Yet. *Regul. Toxicol. Pharmacol.* **2017**, *88*, 214−226.

(7) Mishra, S.; Zhang, W.; Lin, Z.; Pang, S.; Huang, Y.; Bhatt, P.; Chen, S. Carbofuran Toxicity and Its Microbial Degradation in Contaminated Environments. *Chemosphere* **2020**, *259*, No. 127419.

(8) Kabir, E.; Khatun, M.; Nasrin, L.; Raihan, M. J.; Rahman, M. Pure β-Phase Formation in Polyvinylidene Fluoride (PVDF)-Carbon Nanotube Composites. *J. Phys. Appl. Phys.* **2017**, *50* (16), No. 163002.

(9) Majidian, S.; Afsharnia, M.; Taghavi, M.; Kohan, N. A.; Dehghan, A. Photocatalytic Degradation of Methylene Blue Dye Using Bismuth Oxyiodide from Aqueous Solutions. *Int. J. Environ. Anal. Chem.* **2023**, *103* (20), 9519−9531.

(10) Aziz, K. H. H.; Mahyar, A.; Miessner, H.; Mueller, S.; Kalass, D.; Moeller, D.; Khorshid, I.; Rashid, M. A. M. Application of a Planar Falling Film Reactor for Decomposition and Mineralization of Methylene Blue in the Aqueous Media via Ozonation, Fenton, Photocatalysis and Non-Thermal Plasma: A Comparative Study. *Process Saf. Environ. Prot.* **2018**, *113*, 319−329.

(11) Zhi, S.; Tian, L.; Li, N.; Zhang, K. A Novel System of MnO2-Mullite-Cordierite Composite Particle with NaClO for Methylene Blue Decolorization. *J. Environ. Manage.* **2018**, *213*, 392−399.

(12) Sen, T. K.; Afroze, S.; Ang, H. Equilibrium, Kinetics and Mechanism of Removal of Methylene Blue from Aqueous Solution by Adsorption onto Pine Cone Biomass of Pinus Radiata. *Water, Air, Soil Pollut.* **2011**, *218*, 499−515.

(13) Ezugwu, C. I.; Asraf, M. A.; Li, X.; Liu, S.; Kao, C.-M.; Zhuiykov, S.; Verpoort, F. Selective and Adsorptive Removal of Anionic Dyes and CO2 with Azolium-Based Metal-Organic Frameworks. *J. Colloid Interface Sci.* **2018**, *519*, 214−223.

(14) Chen, L.; Ren, X.; Alharbi, N. S.; Chen, C. Fabrication of a Novel Co/Ni-MOFs@BiOI Composite with Boosting Photocatalytic Degradation of Methylene Blue under Visible Light. *J. Environ. Chem. Eng.* **2021**, *9* (5), No. 106194.

(15) Hafeez, A.; Javed, F.; Fazal, T.; Shezad, N.; Amjad, U.-e.-S.; ur Rehman, M. S.; Rehman, F. Intensification of Ozone Generation and Degradation of Azo Dye in Non-Thermal Hybrid Corona-DBD Plasma Micro-Reactor. *Chem. Eng. Process.* **2021**, *159*, No. 108205.

(16) Barros, W. R. P.; Steter, J. R.; Lanza, M. R. V.; Motheo, A. J. Degradation of Amaranth Dye in Alkaline Medium by Ultrasonic Cavitation Coupled with Electrochemical Oxidation Using a Boron-Doped Diamond Anode. *Electrochim. Acta* **2014**, *143*, 180−187.

(17) Januário, E. F. D.; Vidovix, T. B.; de Camargo Lima Beluci, N.; Paixão, R. M.; da Silva, L. H. B. R.; Homem, N. C.; Bergamasco, R.; Vieira, A. M. S. Advanced Graphene Oxide-Based Membranes as a Potential Alternative for Dyes Removal: A Review. *Sci. Total Environ.* **2021**, *789*, No. 147957.

(18) Yagub, M. T.; Sen, T. K.; Afroze, S.; Ang, H. M. Dye and Its Removal from Aqueous Solution by Adsorption: A Review. *Adv. Colloid Interface Sci.* **2014**, *209*, 172−184.

(19) Hokkanen, S.; Bhatnagar, A.; Sillanpää, M. A Review on Modification Methods to Cellulose-Based Adsorbents to Improve Adsorption Capacity. *Water Res.* **2016**, *91*, 156−173.

(20) Sharma, P. K.; Kumar, R.; Singh, R. K.; Sharma, P.; Ghosh, A. Review on Arsenic Removal Using Biochar-Based Materials. *Groundwater Sustainable Dev.* **2022**, *17*, No. 100740.

(21) De Gisi, S.; Lofrano, G.; Grassi, M.; Notarnicola, M. Characteristics and Adsorption Capacities of Low-Cost Sorbents for

https://doi.org/10.1021/acsomega.4c03570
ACS Omega 2024, 9, 30834−30845

Wastewater Treatment: A Review. *Sustainable Mater. Technol.* **2016**, *9*, 10−40.
(22) Ngulube, T.; Gumbo, J. R.; Masindi, V.; Maity, A. An Update on Synthetic Dyes Adsorption onto Clay Based Minerals: A State-of-Art Review. *J. Environ. Manage.* **2017**, *191*, 35−57.
(23) Alam, S.; Ullah, B.; Khan, M. S.; Rahman, N. U.; Khan, L.; Shah, L. A.; Zekker, I.; Burlakovs, J.; Kallistova, A.; Pimenov, N.; Yandri, E.; Setyobudi, R. H.; Jani, Y.; Zahoor, M. Adsorption Kinetics and Isotherm Study of Basic Red 5 on Synthesized Silica Monolith Particles. *Water* **2021**, *13* (20), No. 2803.
(24) Rad, L. R.; Anbia, M. Zeolite-Based Composites for the Adsorption of Toxic Matters from Water: A Review. *J. Environ. Chem. Eng.* **2021**, *9* (5), No. 106088.
(25) Subhan, H.; Alam, S.; Shah, L. A.; Khattak, N. S.; Zekker, I. Sodium Alginate Grafted Hydrogel for Adsorption of Methylene Green and Use of the Waste as an Adsorbent for the Separation of Emulsified Oil. *J. Water Process Eng.* **2022**, *46*, No. 102546.
(26) Gao, Q.; Xu, J.; Bu, X.-H. Recent Advances about Metal−Organic Frameworks in the Removal of Pollutants from Wastewater. *Coord. Chem. Rev.* **2019**, *378*, 17−31.
(27) Santoso, E.; Ediati, R.; Kusumawati, Y.; Bahruji, H.; Sulistiono, D.; Prasetyoko, D. Review on Recent Advances of Carbon Based Adsorbent for Methylene Blue Removal from Waste Water. *Mater. Today Chem.* **2020**, *16*, No. 100233.
(28) Mykhailiv, O.; Zubyk, H.; Plonska-Brzezinska, M. E. Carbon Nano-Onions: Unique Carbon Nanostructures with Fascinating Properties and Their Potential Applications. *Inorg. Chim. Acta* **2017**, *468*, 49−66.
(29) Hu, Y.; Yang, J.; Tian, J.; Jia, L.; Yu, J.-S. Waste Frying Oil as a Precursor for One-Step Synthesis of Sulfur-Doped Carbon Dots with pH-Sensitive Photoluminescence. *Carbon* **2014**, *77*, 775−782.
(30) Gunture; Kaushik, J.; Garg, A. K.; Saini, D.; Khare, P.; Sonkar, S. K. Pollutant Diesel Soot Derived Onion-like Nanocarbons for the Adsorption of Organic Dyes and Environmental Assessment of Treated Wastewater. *Ind. Eng. Chem. Res.* **2020**, *59* (26), 12065−12074.
(31) Venkatesan, R. A.; Balachandran, M. Novel Carbon Nano-Onions from Paraffinum Liquidum for Rapid and Efficient Removal of Industrial Dye from Wastewater. *Environ. Sci. Pollut. Res.* **2020**, *27*, 43845−43864.
(32) Boumediene, M.; Benaïssa, H.; George, B.; Molina, S.; Merlin, A. Effects of pH and Ionic Strength on Methylene Blue Removal from Synthetic Aqueous Solutions by Sorption onto Orange Peel and Desorption Study. *J. Mater. Environ. Sci.* **2018**, *9* (6), 1700−1711.
(33) Mckay, G.; Blair, H.; Gardner, J. The Adsorption of Dyes in Chitin. III. Intraparticle Diffusion Processes. *J. Appl. Polym. Sci.* **1983**, *28* (5), 1767−1778.
(34) Thamer, B. M.; Al-aizari, F. A.; Hameed, M. M. A. Zero-Valent Ni/NiO Core-Shell Nanosheets Supported on Graphene for Highly Efficient Dye Adsorption: Isotherm, Kinetic and Thermodynamic Study. *Chem. Eng. Res. Des.* **2023**, *197*, 656−668.
(35) Araújo, C. S.; Almeida, I. L. S.; Rezende, H. C.; Marcionilio, S. M. L. O.; Léon, J. J. L.; de Matos, T. N. Elucidation of Mechanism Involved in Adsorption of Pb(II) onto Lobeira Fruit (Solanum Lycocarpum) Using Langmuir, Freundlich and Temkin Isotherms. *Microchem. J.* **2018**, *137*, 348−354.
(36) Langmuir, I. The Adsorption of Gases on Plane Surfaces of Glass, Mica and Platinum. *J. Am. Chem. Soc.* **1918**, *40* (9), 1361−1403.
(37) Freundlich, H. M. F. Over the Adsorption in Solution. *J. Phys. Chem. A* **1906**, *57* (385471), 1100−1107.
(38) Jeyakumar, R. P. S.; Chandrasekaran, V. Adsorption of Lead (II) Ions by Activated Carbons Prepared from Marine Green Algae: Equilibrium and Kinetics Studies. *Int. J. Ind. Chem.* **2014**, *5*, No. 2.
(39) Rida, K.; Bouraoui, S.; Hadnine, S. Adsorption of Methylene Blue from Aqueous Solution by Kaolin and Zeolite. *Appl. Clay Sci.* **2013**, *83*−*84*, 99−105.
(40) Liu, L.; Luo, X.-B.; Ding, L.; Luo, S.-L. Application of Nanotechnology in the Removal of Heavy Metal from Water. In *Nanomaterials for the Removal of Pollutants and Resource Reutilization*; Elsevier, 2019; pp 83−147.
(41) Jung, S.; Myung, Y.; Das, G. S.; Bhatnagar, A.; Park, J.-W.; Tripathi, K. M.; Kim, T. Carbon Nano-Onions from Waste Oil for Application in Energy Storage Devices. *New J. Chem.* **2020**, *44* (18), 7369−7375.
(42) Mongwe, T. H.; Matsoso, B. J.; Mutuma, B. K.; Coville, N. J.; Maubane, M. S. Synthesis of Chain-like Carbon Nano-Onions by a Flame Assisted Pyrolysis Technique Using Different Collecting Plates. *Diamond Relat. Mater.* **2018**, *90*, 135−143.
(43) Mohapatra, D.; Badrayyana, S.; Parida, S. Facile Wick-and-Oil Flame Synthesis of High-Quality Hydrophilic Onion-like Carbon Nanoparticles. *Mater. Chem. Phys.* **2016**, *174*, 112−119.
(44) Das, G. S.; Panigrahi, R.; Ghosh, S.; Tripathi, K. M. Waste Frying Oil Derived Carbon Nano-Onions as a Cost-Effective Cathode Material for High-Voltage Zinc-Ion Hybrid Supercapacitors. *Mater. Today Sustainability* **2024**, *25*, No. 100656.
(45) Kumari, P.; Tripathi, K. M.; Awasthi, K.; Gupta, R. Adsorptive Removal of Nitrophenols from Water by Biomass-Derived Carbon Nano-Onions. *Ind. Eng. Chem. Res.* **2023**, *62* (46), 19801−19812.
(46) Tripathi, K. M.; Singh, A.; Bhati, A.; Sarkar, S.; Sonkar, S. K. Sustainable Feasibility of the Environmental Pollutant Soot to Few-Layer Photoluminescent Graphene Nanosheets for Multifunctional Applications. *ACS Sustainable Chem. Eng.* **2016**, *4* (12), 6399−6408.
(47) Raju, K. S.; Das, G. S.; Tripathi, K. M. Nitrogen-Doped Carbon Quantum Dots from Biomass as a FRET-Based Sensing Platform for the Selective Detection of H2O2 and Aspartic Acid. *RSC Sustainability* **2024**, *2* (1), 223−232.
(48) Pyrzyńska, K.; Bystrzejewski, M. Comparative Study of Heavy Metal Ions Sorption onto Activated Carbon, Carbon Nanotubes, and Carbon-Encapsulated Magnetic Nanoparticles. *Colloids Surf., A* **2010**, *362* (1−3), 102−109.
(49) Pathania, D.; Bhat, V. S.; Shivanna, J. M.; Sriram, G.; Kurkuri, M.; Hegde, G. Garlic Peel Based Mesoporous Carbon Nanospheres for an Effective Removal of Malachite Green Dye from Aqueous Solutions: Detailed Isotherms and Kinetics. *Spectrochim. Acta, Part A* **2022**, *276*, No. 121197.
(50) Yadav, B. S.; Dasgupta, S. Effect of Time, pH, and Temperature on Kinetics for Adsorption of Methyl Orange Dye into the Modified Nitrate Intercalated MgAl LDH Adsorbent. *Inorg. Chem. Commun.* **2022**, *137*, No. 109203.
(51) Anastopoulos, I.; Kyzas, G. Z. Agricultural Peels for Dye Adsorption: A Review of Recent Literature. *J. Mol. Liq.* **2014**, *200*, 381−389.
(52) Kausar, A.; Shahzad, R.; Iqbal, J.; Muhammad, N.; Ibrahim, S. M.; Iqbal, M. Development of New Organic-Inorganic, Hybrid Bionanocomposite from Cellulose and Clay for Enhanced Removal of Drimarine Yellow HF-3GL Dye. *Int. J. Biol. Macromol.* **2020**, *149*, 1059−1071.
(53) Zhang, Q.; Zhang, T.; He, T.; Chen, L. Removal of Crystal Violet by Clay/PNIPAm Nanocomposite Hydrogels with Various Clay Contents. *Appl. Clay Sci.* **2014**, *90*, 1−5.
(54) Shaik, S. A.; Roy, U.; Sengupta, S.; Goswami, A. Adsorption of Safranin O on Halloysite Nanotubes: A Mechanistic Case Study for Efficient Wastewater Remediation. *Int. J. Environ. Sci. Technol.* **2023**, *20* (5), 5405−5426.
(55) Safarzadeh, H.; Peighambardoust, S. J.; Mousavi, S. H.; Foroutan, R.; Mohammadi, R.; Peighambardoust, S. H. Adsorption Ability Evaluation of the Poly (Methacrylic Acid-Co-Acrylamide)/Cloisite 30B Nanocomposite Hydrogel as a New Adsorbent for Cationic Dye Removal. *Environ. Res.* **2022**, *212*, No. 113349.
(56) Ngulube, T.; Gumbo, J.; Masindi, V.; Maity, A. Preparation and Characterisation of High Performing Magnesite-Halloysite Nanocomposite and Its Application in the Removal of Methylene Blue Dye. *J. Mol. Struct.* **2019**, *1184*, 389−399.
(57) De Benedetto, C.; Macario, A.; Siciliano, C.; Nagy, J. B.; De Luca, P. Adsorption of Reactive Blue 116 Dye and Reactive Yellow 81 Dye from Aqueous Solutions by Multi-Walled Carbon Nanotubes. *Materials* **2020**, *13* (12), No. 2757, DOI: 10.3390/ma13122757.

https://doi.org/10.1021/acsomega.4c03570
ACS Omega 2024, 9, 30834−30845

(58) Cazetta, A. L.; Pezoti, O.; Bedin, K. C.; Silva, T. L.; Paesano, A., Junior; Asefa, T.; Almeida, V. C. Magnetic Activated Carbon Derived from Biomass Waste by Concurrent Synthesis: Efficient Adsorbent for Toxic Dyes. *ACS Sustainable Chem. Eng.* **2016**, *4* (3), 1058−1068.
(59) Salem, A.-N. M.; Ahmed, M.; El-Shahat, M. Selective Adsorption of Amaranth Dye on Fe3O4/MgO Nanoparticles. *J. Mol. Liq.* **2016**, *219*, 780−788.
(60) Noreen, S.; Mustafa, G.; Ibrahim, S. M.; Naz, S.; Iqbal, M.; Yaseen, M.; Javed, T.; Nisar, J. Iron Oxide (Fe2O3) Prepared via Green Route and Adsorption Efficiency Evaluation for an Anionic Dye: Kinetics, Isotherms and Thermodynamics Studies. *J. Mater. Res. Technol.* **2020**, *9* (3), 4206−4217.
(61) Oladejo, J.; Shi, K.; Chen, Y.; Luo, X.; Gang, Y.; Wu, T. Closing the Active Carbon Cycle: Regeneration of Spent Activated Carbon from a Wastewater Treatment Facility for Resource Optimization. *Chem. Eng. Process.* **2020**, *150*, No. 107878.
(62) Saratale, R. G.; Sun, Q.; Munagapati, V. S.; Saratale, G. D.; Park, J.; Kim, D.-S. The Use of Eggshell Membrane for the Treatment of Dye-Containing Wastewater: Batch, Kinetics and Reusability Studies. *Chemosphere* **2021**, *281*, No. 130777.
(63) Ogunlaja, A.; Nwankwo, I. N.; Omaliko, M. E.; Olukanni, O. D. Biodegradation of Methylene Blue as an Evidence of Synthetic Dyes Mineralization during Textile Effluent Biotreatment by Acinetobacter Pittii. *Environ. Processes* **2020**, *7*, 931−947.
(64) Sonwani, R. K.; Jaiswal, R. P.; Rai, B. N.; Singh, R. S. Moving Bed Biofilm Reactor-(MBBR-) Based Advanced Wastewater Treatment Technology for the Removal of Emerging Contaminants. In *Development in Wastewater Treatment Research and Processes*; Elsevier, 2022; pp 349−370.

https://doi.org/10.1021/acsomega.4c03570
ACS Omega 2024, 9, 30834−30845